International Journal of Biological Macromolecules 141 (2019) 831–842

Contents lists available at ScienceDirect

International Journal of Biological Macromolecules

journal homepage: http://www.elsevier.com/locate/ijbiomac

Generalized kinetics for thermal degradation and melt rheology for poly (lactic acid)/poly (butylene succinate)/functionalized chitosan based reactive nanobiocomposite

Monika, Neha Mulchandani, Vimal Katiyar *

Department of Chemical Engineering, Indian Institute of Technology Guwahati, Guwahati, 781039, Assam, India

ARTICLE INFO

Article history:
Received 24 June 2019
Received in revised form 6 September 2019
Accepted 7 September 2019
Available online 09 September 2019

Keywords:
Thermal degradation kinetic
Generalized mechanism plots
Melt rheology

ABSTRACT

Systematic kinetics of melt-blended Poly(lactic acid) (PLA)/Poly(butylene succinate) (PBS) and PLA/PBS/functionalized chitosan (FCH) nanobiocomposites with dicumyl peroxide (DCP) and chemical changes thereof at degradation temperatures are evaluated using thermogravimetry (TGA) and thermogravimetry coupled to Fourier transform infrared spectroscopy (TGA–FTIR). A comprehensive kinetic model is employed on above blended samples, including (i) Flynn–Wall–Ozawa, Kissinger, Kissinger–Akahira–Sunose methods to investigate the kinetic and thermodynamic variables, and (ii) Generalized master plots to propose the thermal-induced mechanism. The thermal stability of PLA/PBS reduced with increasing FCH loading up to 3 wt%, and improved for DCP treated PLA/PBS/1FCH at maximum degradation temperature (T_{max}) is noticed. The activation energy estimated from Flynn-Wall-Ozawa method are (129–139 $kJmol^{-1}$), (116–152 $kJmol^{-1}$), (109–146 $kJmol^{-1}$), (132–169 $kJmol^{-1}$) and (120–166 $kJmol^{-1}$) for PLA/PBS, PLA/PBS/1FCH, PLA/PBS/3FCH, PLA/PBS/1DFCH and PLA/PBS/3DFCH respectively. The generalized master plots depicts that the PLA/PBS blend exhibited L2–F1 mechanism whereas their nanobiocomposite with or without DCP followed L2–D_n and A2–L2–D_n mechanism respectively. Coupled TGA–FTIR highlights the similar kinds of products such as lactide, acetaldehyde, esters, CO_2 and CO liberated during the thermal degradation of PLA/PBS blend and their nanobiocomposites. These crosslinked/branched structures are postulated by the rheological behavior which confirmed increase in the complex viscosity (η^*) and storage modulus (G′) of PLA/PBS/D/1FCH.

1. Introduction

Due to economic and environmental concerns, the quest for development of renewable bio-based material as the potential replacement for synthetic polymer based packaging is an emerging area for manufacture and scientist [1]. In past, some bio-based and biodegradable polymers such as the poly lactic acid (PLA), poly (butylenes succinate) (PBS), polycaprolactone (PCL), Polybutylene adipate-*co*-terephthalate (PBAT) were prologue in the commercial market [2]. Among the entire biopolymer family, PLA has seen a notable surge of research concern due to its easy process ability, biocompatibility and properties comparable to many commodity plastic [3,58]. In spite of various significant characteristics, it shows some limitation such as brittle nature, low thermal stability, narrow processing window and poor melt strength [4]. However, these limitation causes worthwhile industrial challenges and inadequate for large scale applications [4,57].

Among the diversity of approaches, blend of PLA with other biopolymers such as PBS is a good choice to tailor the properties such as toughness [5]. Despite this interest, PLA/PBS blend has limited application because requirements of many products are not satisfied due to poor melt strength and barrier properties. Therefore, various strategies have been developed in order to overcome these limitations. One possible approach is an incorporation of inexpensive bio-filler in polymer blend [6]. Moreover, this perspective shows fabrication of nanobiocomposite from biofiller with PLA/polyester blend for commercially viable applications.

Chitosan (CH) is a typical cationic polysaccharide, produced by deacetylation of chitin, which utilized due to its antimicrobility, biodegradability, bio compatibility, and non toxicity [7–9]. It attains much awareness in wide applications such as wastewater treatment, biomedicine and agricultural sectors. Applications of chitosan are limited due to its solubility and hydrophilic nature in packaging sectors. To solve this issue, chitosan can be chemically modified by grafting some other hydrophobic oligomer or biopolymer to convert into hydrophobic nature using one pot synthesis in absence of solvent or catalyst. Hence, dispersion of chitosan in hydrophobic PLA phase can also be enhanced by the functionalized chitosan (FCH) [10].

In this work, DCP plays a role as a cross-linking agent [11] to modify the properties of PLA/PBS/FCH based system in order to develop the

* Corresponding author.
E-mail address: vkatiyar@iitg.ernet.in (V. Katiyar).

https://doi.org/10.1016/j.ijbiomac.2019.09.058
0141-8130/

nanobiocomposites with balanced thermo-mechanical characteristics. Melt extrusion is one of the promising techniques for the development of polymeric nanobiocomposites. In general, polymeric materials such as PLA and PBS are susceptible to thermal decomposition at high temperature, which assists in the reduction of properties due to the severe mass loss. The probable reason for mass loss is the evolution of small volatile fragments after autocatalytic degradation [12].

TGA is the most accepted tool for calculating the thermal stability, degradation kinetic triplets such as activation energy (E_a), rate constant (k) and pre-exponential factor (A) [13]. For the systematic investigation, nonisothermal kinetic modeling helps for the better understanding of the decomposition behavior of all the systems and conducted a quantitative result from the TGA data. Moreover, kinetic parameters are estimated using Kissinger, Flynn Wall Ozawa (FWO) and Kissinger Akhaira Sunose (KAS) methods. TGA–FTIR technique is further utilized to study the release of gas species during the decomposition process. Also, a study evaluated the influence of FCH with or without DCP on the thermal behavior of PLA/PBS based nanobiocomposite, which is important to determine how nanobiocomposites processed without suffering serious thermal decomposition to make it feasible at an industrial level. Further, rheological properties are beneficial in the detailed investigation of structure vs. property relationship of polymer nanobiocomposites which plays an essential role in effective processing during the molten state. Measurements of rheological characteristics under shear are utilized to analyze the interaction between the polymer and filler during the molten state. For better understanding of structural-properties relationship, rheological response is investigated to observe the tailored flow characteristics of nanobiocomposite by modifying the molecular architecture through reactive extrusion with DCP, as well as altering the resultant properties of the system [57]. Srimalanon et al. (2018) reported that influence of HPQM (2 hydroxypropyl 3 piperazinyl quinoline carboxylic acid methacrylate) as a commercial biocide and DCP on the antimicrobial, mechanical and rheological properties of DCP treated PLA/PBS blend via reactive extrusion [59].

The perspective of this research is to explore the rheological and thermal performance evaluation of DCP treated PLA/PBS/FCH nanobiocomposites with potential utilization in the packaging sector, by means of TGA kinetics, hyphenated TGA–FTIR and melt rheology.

2. Theoretical considerations for kinetic computations

To investigate the TG kinetics of polymeric system, thermal decomposition process is considered as irreversible type of reaction. Thermogravimetric analysis (TGA) is beneficial thermal technique to investigate the degradation kinetics parameters and mechanism [14]. TGA data at dynamic heating regime has been analyzed using model-free kinetic approach to speculate the effect of FCH on PLA/PBS blend with or without DCP. Generally, the kinetics practice of polymer decomposition can be demonstrated using the following rate Eq. (1) which is mentioned in Ref. [15]:

$$\frac{d\alpha}{dt} = k(\mathrm{T})\ \mathrm{f}(\alpha) = A\ \exp\left(\frac{-E_a}{RT}\right)\mathrm{f}(\alpha) \tag{1}$$

where α means the extent of conversion, $\frac{d\alpha}{dt}$ indicates the decomposition rate, k(T) expressed the temperature based rate constant and f(α) denotes the typical differential expression of various kinetic model functions, which relies on specific decomposition mechanism. A is the pre-exponential factor (s^{-1}), T is the absolute temperature (K), R for the universal gas constant (J mol^{-1} K^{-1}) and E_a is the activation energy (kJ mol^{-1}). It can be defined by the given expression in Eq. (2):

$$\alpha = \frac{(w_o - w_t)}{(w_o - w_r)} \tag{2}$$

where w_o is the initial weight, w_t is the weight at time t and w_r is the residual weight of the samples.

For non-isothermal TGA kinetic study, substituting the heating rate (β = dT/dt) and rearranging the Eq. (1), one can get the Eq. (3) in which the temperature-dependent degradation rate defined as follows which was shown by Ref. [16]:

$$\left(\frac{d\alpha}{dT_i}\right) = \frac{A}{\beta_i}\exp\left(\frac{-E_a}{RT_i}\right)f(\alpha) \tag{3}$$

and

$$g(\alpha) = \frac{A}{\beta_i}\int_0^T \exp\left(\frac{-E_a}{RT_i}\right)dT \tag{4}$$

Eq. (4) incapable to solve using analytical solution and it can be rewritten as [17]:

$$g(\alpha) = \frac{AE}{R\beta_i}\left[\exp\frac{(-x)}{x} - \int_x^{\infty}\exp\left(\frac{-x}{x}\right)dx\right] = \frac{AE}{R\beta_i}p(x) \tag{5}$$

where x (= E_a/RT) is the reduced activation energy. The function p (x) can be changed by different approximations. In order to evaluate these parameters, models with various assumptions has been suggested to simplify the complexity of the decomposition process. Generally model free kinetic study is selected where the validity of determination of transformation rate is limited or where some unreliability over baseline of the TG data exits, as compared to other models. Model free (FWO, KAS and Kissinger) methods can provide the most reliable approach for the estimation of E_a of polymeric system.

2.1. Flynn Wall Ozawa (FWO) method

FWO is an integral isoconversional method which quantifies the distribution of E_a as α without prior comprehension to decomposition mechanism [18,19]. This method is utilized for TGA kinetic interpretations of complex degradation mechanism. Using Doyle's approximation ($lnp(x) \cong -5.3305 - 1.025x$), this data can be integrated and solution of integration after logarithms is represented in Eq. (6) which is valid for (20 ≤ x ≤ 60) [20].

$$log\beta_i = \left\{ log\frac{AE_a}{g(\alpha)R} - 2.315\right\} - \frac{0.457E_a}{RT_i} \tag{6}$$

The distribution of E_a with α can be estimated based on the slope (= 0.457 E_a/RT_i) of the straight line.

2.2. Kissinger-Akahira-Sunose (KAS) method

KAS method is also known as an integral isoconversional method. With the help of Eq. (7), we can calculate the distribution of E_a with α. The approximation $p(x) \cong \frac{e^{-x}}{x^2}$ utilized to solve the Eq. (5), which reliable for (20 ≤ x ≤ 60) [21,22].

$$\ln\left(\frac{\beta_i}{T_i^2}\right) = -\left(\frac{E_\alpha}{RT_i}\right) + \ln\left(\frac{AR}{Eg(\alpha)}\right) \tag{7}$$

The E_a can be determined from the slope (E_a/R) of a graph of ln (β/T_i^2)) against $-1/T_i$ for given extent of conversion (α).

2.3. Kissinger method

Kissinger method is depending on the model-free approach where no requirement to evaluate E_a for each α in order to obtain thermal kinetic parameters (E_a, A) with relatively high accuracy [23,24]. This method adopted the calculation of E_a at T_m, got from the slope (E_a/R)

of the lines and used the following Eq. (8):

$$\ln\left(\frac{\beta_i}{T_m^2}\right) = -\frac{E_a}{RT_m} + \ln\left(\frac{AR}{E_a}\right) \tag{8}$$

where T_m is the maximum degradation temperature.

2.4. Established master plots

The established kinetic equation proposed by Ozawa [25] is utilized to interpret the master plots that show validity for the experimental plots obtained under any heating rate [26]. Thus, reduced time (θ) is defined by Eq. (9) [27]:

$$\theta = \int_0^t \exp\left(-\frac{E_a}{RT}\right)dt \tag{9}$$

where considering the integral of Eq. (1), it can be mentioned that θ indicated the time required to attain a specific value of α at infinite T. The following expression can be obtained by differentiating Eq. (9):

$$\frac{d\theta}{dt} = \exp\left(-\frac{E_a}{RT_i}\right) \tag{10}$$

After a combination of Eq. (1) and Eq. (10), the following Eq. (11) is got

$$\frac{d\alpha}{d\theta} = Af(\alpha) \tag{11}$$

This can be rearranged, as described in Eq. (12),

$$\frac{d\alpha}{d\theta} = \frac{d\alpha}{dt}\exp\left(-\frac{E_a}{RT_i}\right) \tag{12}$$

where $\frac{d\alpha}{d\theta}$ related to the generalized reaction rate.

According to the differential form of the generalized kinetic equation, the relationship between the experimentally obtained data and generalized kinetic rate can be accomplished, using α at 0.5 (reference point), from Eq. (13):

$$\frac{d\alpha/d\theta}{(d\alpha/d\theta)_{0.5}} = \frac{d\alpha/dt}{(d\alpha/dt)_{0.5}}\frac{exp(E_\alpha/RT_i)}{exp\,(E_\alpha/RT_{0.5})} \tag{13}$$

Thus, $T_{0.5}$ denotes the reaction temperature where α is 0.5.

The master plots of degradation mechanisms listed in Table S1 and can be determined according to Eq. (14):

$$\frac{d\alpha/d\theta}{(d\alpha/d\theta)_{0.5}} = \frac{f(\alpha)}{f(0.5)} \tag{14}$$

Thereafter, the master plots has been compared with the experimental plot for obtaining the mechanism of the decomposition process under any heating rate, Eq. (14) should be reliable for the analysis of TG data. Further, it is independent of the temperature profiles under which they are obtained [28]. Derivation for master plots using random scission analysis is discussed in section S5.

As displayed in Table S1, the algebraic expressions that shows the degradation mechanism of polymers divided into five categories: nuclei formation and growth (A_n), reaction mechanism controlled by the surface (R_n), diffusion phenomena depend on heat transfer (D_n), random degradation of nuclei (F_n) and random chain scission (L_n) for thermal decomposition process [28,30].

2.5. Determination of thermodynamic parameters

Determination of the thermodynamic parameter such as entropy (ΔS), enthalpy of activation (ΔH), Gibbs free energy (ΔG) using the following Eqs. (15) to (17) respectively [29,31]

$$\Delta S = R\left[\ln\left(\frac{Ah}{kT}\right)\right], \tag{15}$$

$$\Delta H = E_a - RT, \tag{16}$$

$$\Delta G = \Delta H - T\Delta S, \tag{17}$$

where h and k is the Planck and Boltzmann constant respectively.

3. Experiments

3.1. Materials

Poly L-lactic Acid (PLA) 4032D with number average molecular weight (MW) and polydispersity index (M_n ~150,000 D_a and PDI ~1.3) supplied from Nature works (USA). Polybutylene Succinate (PBS) 1001MD with M_n ~88,000 D_a, PDI~2.2 is obtained from Showa Highpolymer, Japan. Dicumyl Peroxide (DCP), supplied by Sigma Aldrich (India), utilized as crosslinking agent. L-lactic acid and medium MW Chitosan with degree of deacetylation >70% supplied from Sigma Aldrich to synthesize functionalized chitosan. Whatmann® filter paper (grade: 1) is used for vacuum filtration of the functionalized chitosan (*F*CH) to remove the unreacted part. Acetone (Emplura) is purchased from Merck, India.

3.2. Synthesis of functionalized chitosan (FCH)

FCH is synthesized using microwave-based reactor as prior art published earlier [10]. Both lactic acid and chitosan are manually mixed (~ratio of 3.33:1 wt/wt%) and kept into the round bottom flask (RBF). Thereafter lactic acid is soaked into chitosan to enhance the yield for 12 h and this mixture is placed in microwave reactor under the inert atmosphere. The condenser is connected with RBF and clamped outside microwave to obtain byproducts which can easily accumulate in an attached reservoir. The condenser should be covered by a heating belt to prevent the condensation of byproducts. The possible change in structure is assessed from the FTIR and ^{1}H NMR analysis as mentioned in Fig. S1 (a) and (b) respectively. Condensation polymerization is executed at 110 °C, 240 watts for half an hour to obtain a low molecular weight (M_n ~1400 Da and M_w ~3000 Da) dark brown viscous product due to the grafting of lactic acid on chitosan backbone to produce oligo-L lactic acid functionalized chitosan (FCH). As seen in Fig. S1 (e), moleculare weight is confirmed through the GPC analysis. The reaction pathway on the basis of FTIR and ^{1}HNMR spectroscopy is displayed below in Fig. 1, as supported by earlier report [10]:

The fixed amount of FCH was mixed in acetone (~20 ml) with magnetic stirring at 1000 rpm for 6 h at ambient conditions. The solution was filtered with Whatman filter paper (pore size ~0.45 μm) with a vacuum filtration method to remove all ungrafted chitosan or lactic acid and other insoluble impurities.

3.3. Fabrication of PLA/PBS based reactive nanobiocomposites via melt extrusion

Pellets of PLA and PBS are dried under vacuum at a set temperature of 40 °C overnight to make moisture free. Acetone (10 ml) is added into DCP (1phr) and sprayed on PLA/PBS (80/20 wt%) blend. Further, DCP coated PLA–PBS blend is manually mixed with 1 and 3 wt% loading of FCH and vacuum drying is essential to remove the trapped acetone. PLA–PBS–*F*CH batches with or without DCP are melt-mixed using twin

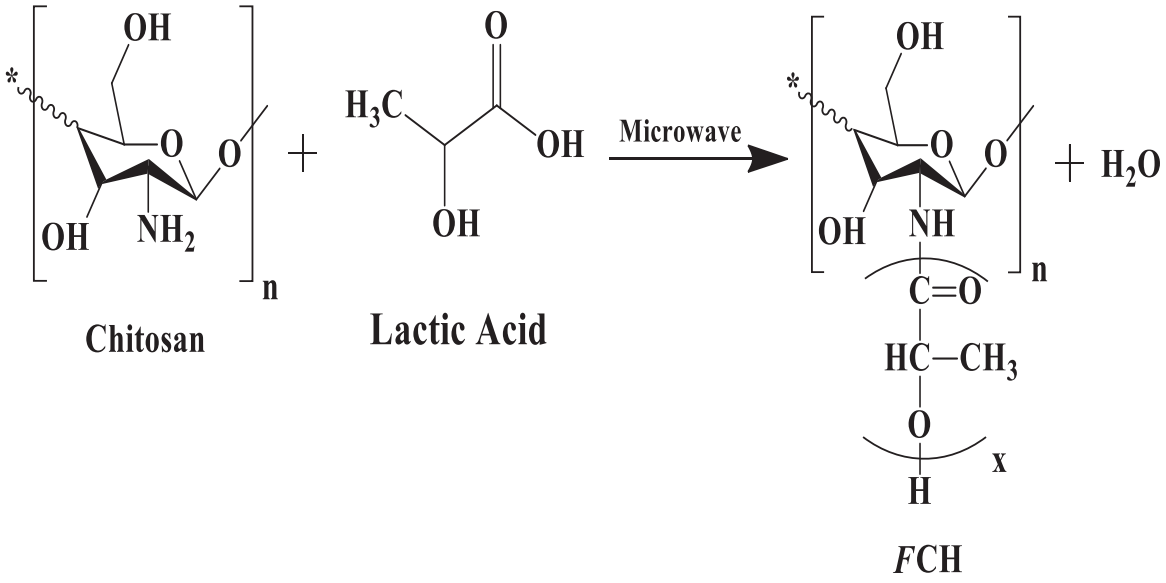

Fig. 1. (a) Reaction pathway for the synthesis of FCH confirmed using (b) FTIR (c) ^{1}H NMR analysis.

extruder (Haake Mini Lab II, Thermofisher Scientific), processing parameters are fixed such as temperature 185 °C and screw speed 60 rpm for ~300 s. Finally, batches of PLA/PBS (80/20) based nanobiocomposites are marked as PLA/PBS/1FCH (80/20/1), PLA/PBS/3FCH (80/20/3), PLA/PBS/1DFCH (80/20/1/1) and PLA/PBS/3DFCH (80/20/1/3) respectively.

3.4. Method of study

Field emission transmission electron microscopy (FETEM, JEOL-2100, and USA) is used to evaluate the phase morphology. The samples are prepared in chloroform (grade HPLC) followed by magnetic stirring for minimum 2 h to obtain uniform dispersion.

Thermal stability and kinetic parameters of PLA/PBS blend and their nanobiocomposites calculated by thermal gravimetric analysis (TGA 4000, Perkin Elmer, and USA) in order to get more insight into its decomposition behavior. The measurement is carried out at 30 to 600 °C at the various heating rate of 5, 10, 15 and 20 min^{-1} under N_2 atmosphere.

Hyphenated TGA 4000–FTIR (Frontier, Perkin Elmer, USA) is an established technique for investigating the thermal decomposition behaviour of polymer. During the TGA-FTIR run, the major volatile components released from the TGA, are captured in the FTIR cell window and record the IR spectra in continuous mode. Both the cell window and transfer line (TL 8000) are heated at 260 °C to circumvent the condensation of volatile species and the IR spectra are scanned in the wave number range (4000–450 cm^{-1}) with resolution of 4 cm^{-1}.

Rheological properties are determined using an interfacial rheometer (Anton Par MCR 301), a parallel plate (diameter 25 mm) at 190 °C. Experiments are performed in the linear viscoelastic region, and strain rate (~5%) is applied. For PLA/PBS blend and their nanobiocomposites, measurements are performed using dynamic frequency sweep mode (frequency range ~ 0.1 to 600 rad/s).

4. Result and discussion

4.1. FETEM analysis

Fig. 2 displays FETEM micrographs of FCH; PLA/PBS/FCH based nanobiocomposite with and without DCP at higher magnification. The light spherical domains depict in Fig. 2(b)–(c) are PBS inclusions, whereas the dark spherical spots confirm the presence of FCH nanoparticles. As observed, size of FCH nanoparticles are reduced after addition of DCP into PLA/PBS/FCH based bionanocomposites.

4.2. (TGA) analysis

From the TGA analysis, the thermal stability in terms of the temperature for 15% weight loss temperature (T_{15}), 50% weight loss temperature (T_{50}) and maximum degradation temperature (T_{max}) are mentioned in Table 1. TGA is done to investigate the thermal decomposition behavior of FCH, PLA, PLA/PBS blend and their PLA/PBS/FCH nanobiocomposite with or without DCP. TGA of FCH, PLA is mentioned in Fig. S1 (c) and Fig. S2 (a) respectively. Fig. 3(a)–(b) confirms TGA and first derivative thermograms (DTG) plots of PLA/PBS and their nanobiocomposites with or without DCP and their quantified parameters are displayed in Table 1. All of the samples showed two-stage degradation process, revealed from the DTG. Although the incorporation of 1 wt% FCH into PLA/PBS blend shows no significant reduction in T_{15} and T_{max} and it varied insignificant in comparison to PLA/PBS blend which may be due to improve compatibility between the PLA and PBS phase in presence of 1 wt% FCH. Further increasing the FCH loading with 3 wt%, nanobiocomposite displays the reduction in thermal parameters. The possible reason behind this is the increase in short OLLA chain attached with chitosan offers plasticization effect and finally supported the thermal decomposition of nanobiocomposite at lower temperature [10,32]. For DCP treated PLA/PBS/1FCH, maximum degradation temperature (T_{max}) is shifted to the higher temperature while no significant change in 15% wt. loss temperature (T_{15}) observed in comparison to PLA/PBS/1FCH nanobiocomposite. This result could be ascribed that the thermal stability is slightly improved due to the development of the branching/cross-linking sites at the interface of polymers which trying to control the decomposition process at higher temperature [33,34].

4.3. Non-isothermal degradation kinetics

The influence of different loading of FCH (1 and 3 wt%) on the PLA/PBS in the presence of DCP is systematically investigated using non-isothermal TGA kinetics. The TGA and DTG plots of PLA/PBS blend and their nanobiocomposites plotted at different heating rates (5, 10, 15 and 20°) are illustrated in Fig. S2 (a)–(f). It is well-known fact that the mass loss plot shifts to the right due to less retention time at the higher heating rate and vice versa [35]. Moreover, the kinetic parameters are

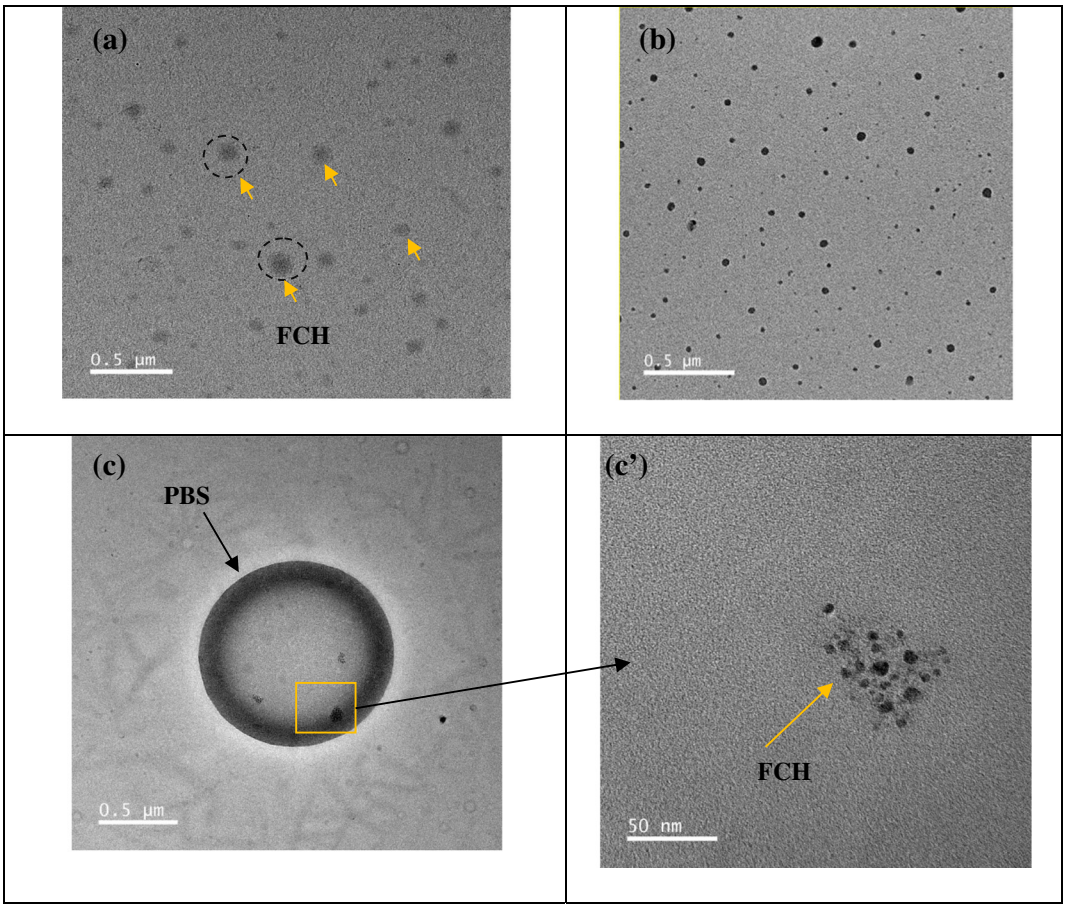

Fig. 2. FETEM analysis of FCH (a), PLA/PBS/1DFCH (b) and enlarge image of PLA/PBS/1DFCH (c)–(c').

calculated by the widely used model-free methods such as Kissinger, FWO and KAS method.

4.4. Estimation of apparent E_a

Analytical methods are utilized to determine the E_a from TGA data, which already described in theoretical approach. The FWO ($\log \beta_i$ vs$1000/T_i$) and KAS ($\ln \beta_i/T_i^2$ vs $1000/T_i$) plots for PLA, PLA/PBS blend, PLA/PBS/FCH nanobiocomposites with or without DCP were displayed in Fig. S3 (a) – (f) and S4 (a) – (f) respectively; the slope of linear fit is utilized to estimate the E_a. Notably, the linear fit corresponding to α range (0.1–0.9), indicates that both the isoconversional methods are appropriate to the analyzed system.

For all the samples, the distribution of E_a against α shows in Fig. 4 (a) and (b) respectively; and summarize in Table 2. Moreover, similar values of E_a are observed from methods within experimental uncertainty using isoconversional methods. When the E_a is remained unchanged for the various conversion degrees, the single step mechanism involved. The variation of E_a with α is sign of multiple reactions; since many reactions are further involved with increase in temperature. From Fig. 3, it can be noticed that the value of E_a varied with α in case of PLA. Therefore, decomposition behaviour of PLA is not processed by simple phenomena because of several reactions occurred concurrently. In general, PLA decomposition occurred by the cleavage of the ester group and chain scission of typical C—C and C—O bond on the backbone chain. It has been suggested that PLA chains undergo degradation by hydrolysis due to the presence of the trace of water, the presence of cyclic oligomer due to the intermolecular transesterification reaction, acrylic acid, acetaldehyde, and CO_2 produced due to cis-elimination and fragmentation respectively [36,37,39].

For PLA/PBS blend, the determined value of E_a is ~129 kJ mol^{-1} at the initial level. It suggests less energy is needed to bond scission at a primary stage to commence the decomposition process, due to the existence of the more active sites at the polymer chain ends. It is observed that the E_a remained unchanged at the conversion range (0.2–0.7) and slightly decreased after it which subsequently led to the participation of two mechanisms in this case. The probable reason can be recommended that the blend morphology and the comparatively poor interaction between the PLA and PBS phase, somehow varied the energy needed for the decomposition of each of the components.

For PLA/PBS/1FCH nanobiocomposite, the dependence on E_a can be separated into three distinct regions. It shows remarkable improvement in E_a up to ~153 kJ mol^{-1} in the first (I) region with increasing α~0.3, estimated value of E_a change slowly in the second (II) region ($0.3 \leq \alpha \geq 0.7$), this stage corresponding to the depolymerisation and deacetyaltion of chitosan. From the third (III) region, it is observed that the slight enhancement in value of E_a is noticed and almost remained constant due to the residual crosslinked degradation chitosan.

Table 1
Influence of reactive modification on thermal stability of PLA/PBS based ternary nanobiocomposites.

Samples	T_{15} (°C)	T_{max} (°C)	T_{50} (°C)
PLA	353	376	371
PLA/PBS	349	371	368
PLA/PBS/1FCH	347	369	366
PLA/PBS/3FCH	343	365	361
PLA/PBS/1DFCH	346	373	370
PLA/PBS/3DFCH	345	371	369
FCH	241	306	300

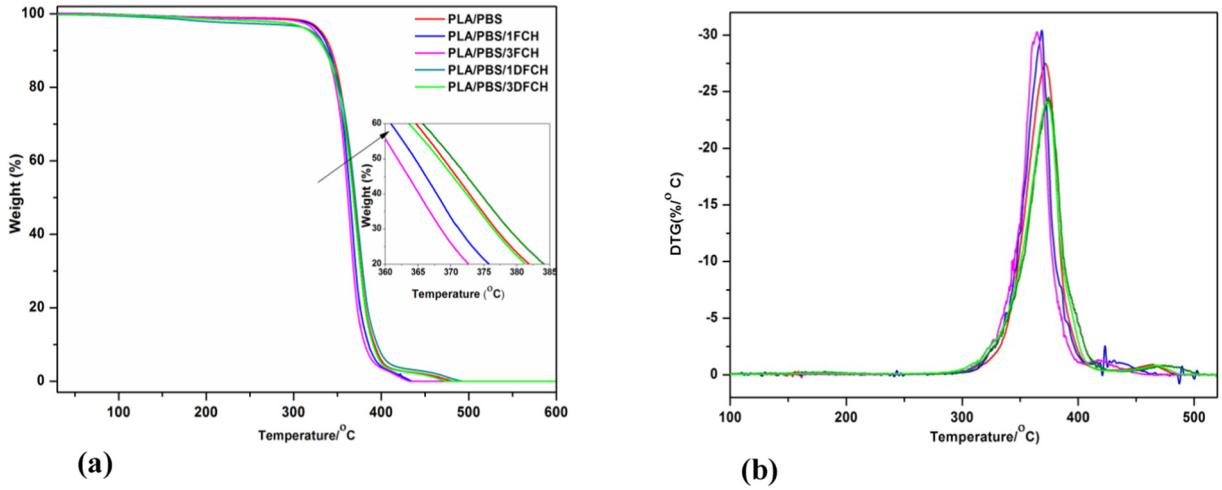

Fig. 3. (a)–(b) TGA, DTG of the PLA/PBS based ternary system without and with DCP content.

This confirms that it promotes the decomposition process which involves at least three distinct types of mechanisms. As evidence, calculated E_a of PLA/PBS/FCH based nanobiocomposites is lower than PLA/PBS blend. Similar trend is also noticed in case of PLA/PBS/3FCH nanobiocomposite. This means that less energy is necessary due to the availability of more active terminal sites which subsequently led to enhance the auto-catalytic effect during the thermal decomposition of polymer nanobiocomposite. It is probably due to that the anhydrous chitosan produced by the dismissal of bound, unbound water during degradation; which produced more H^+ ions. The higher concentrations of H^+ ions also enhance the chain scission of ester groups in the random fashion for polymer nanobiocomposite [10,40]. There is a major possibility that the developed intermediates further face the random chain scission type decomposition which is probably due to hydrolysis of ester group at the chain ends [10,40,41]. Therefore, thermal consistency is reduced to increase in the FCH loading in polymer nanobiocomposite.

For DCP treated PLA/PBS/1FCH nanobiocomposite, it is observed that the E_a is gradually enhanced with α. Such variation in value of E_a is related to the multi-stage decomposition process [42]. This result shows that the delayed thermal decomposition of polymer nanobiocomposite due to inducing branching/crosslinking effect [33,43]. This can be further explained that more energy input is required to cleavage the new C—C linkage.

For DCP treated PLA/PBA/3FCH, slight decrement in E_a is observed as compared to PLA/PBS/1DFCH which is due to the possible reduction in the extent of branching/crosslinking linkage in the system. From the Fig. 4, it is clear that the more than two different types of mechanism are deployed in order to explain the decomposition behaviour for DCP treated PLA/PBS/1FCH and PLA/PBS/3FCH nanobiocomposite.

For the Kissinger method, the smooth relativity of the linear fits affirms the feasibility of this method [44], as clearly seen in Fig. 5. Comparing the obtained E_a from the Kissinger method is higher than FWO and KAS method, which is due to different approximation utilized to solve the methods.

4.5. Calculation of thermodynamic variables

Thermodynamic variables such as ΔG, ΔS and ΔH are obtained at T_{max} using the Kissinger method for all the samples, as mentioned in Table 3. As the calculated value of ΔG, ΔH found positive while ΔS shows negative sign. The positive value of ΔH suggests that the possible decomposition processes are endothermic in nature and confirms that bond dissociation increase with increase in temperature. For all the samples, a positive sign of ΔG indicates the bond dissociation processes are non-spontaneous at T_{max}. The negative sign of ΔS confirmed that the activated complex produced at higher temperature.

4.6. Generalized method for predicting degradation mechanism

Generalized experimental plots determined on the basis of Eq. (9) are displayed in Fig. 5 and precisely assisted the prediction of the mechanism by comparing it with the master plot. The kinetic parameters

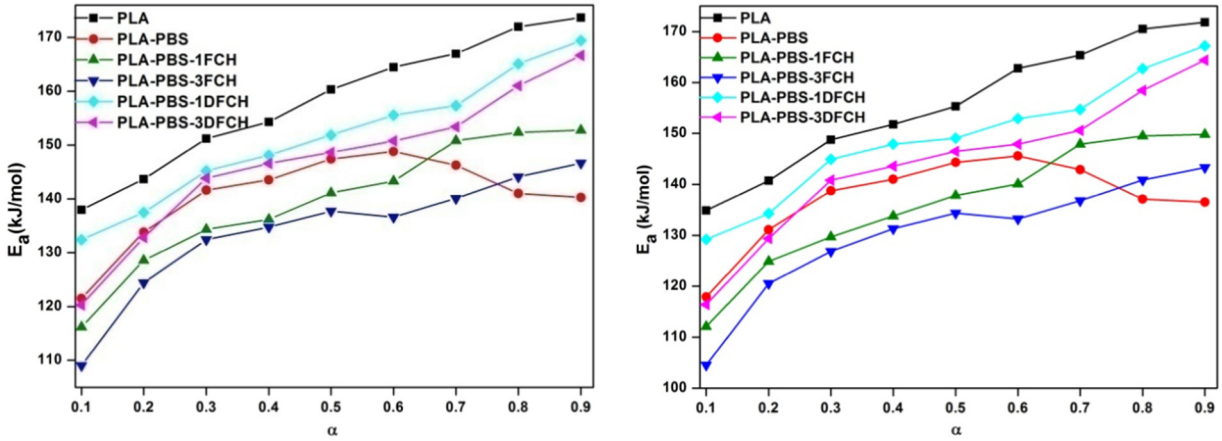

Fig. 4. Activation energy (E_a) vs. conversion (α) profiles for PLA/PBS and their bionanocomposites with or without DCP using (a) FWO (b) KAS methods.

Table 2
Estimated apparent E_a with regression coefficient (R^2) for PLA, PLA/PBS blend, and their nanobiocomposite obtained using FWO, KAS and Kissinger methods.

Samples	FWO model			KAS model			Kissinger	
	E_a (0.1–0.9)	E_a	R^2	E_a (0.1–0.9)	E_a	R^2	E_a	R^2
PLA	137–173	158	0.994	134–171	156	0.996	162	0.999
PLA/PBS	129–139	140	0.995	117–136	136	0.996	144	0.999
PLA/PBS/1FCH	116–152	139	0.995	112–149	135	0.993	142	0.998
PLA/PBS/3FCH	109–146	133	0.994	104–143	130	0.993	137	0.994
PLA/PBS/1DFCH	132–169	151	0.997	129–167	148	0.997	152	0.999
PLA/PBS/3DFCH	120–166	147	0.996	116–164	144	0.995	146	0.995

Table 3
Thermodynamic variables for PLA, PLA/PBS blend and their nanobiocomposite calculated using the Kissinger method.

Samples	Thermodynamic variables			
	A (s^{-1})	ΔH ($kJmol^{-1}$ K^{-1})	ΔS ($kJmol^{-1}$)	ΔG ($kJmol^{-1}$)
PLA	5.52E+12	156.80	-0.40900	157.06
PLA/PBS	1.98E+11	144.79	−0.14055	235.3
PLA/PBS/1FCH	5.75E+13	167.59	−0.11062	238.6
PLA/PBS/3FCH	1.90E+13	161.20	−0.11727	236.1
PLA/PBS/1DFCH	9.57E+13	170.95	−0.10707	240.1
PLA/PBS/3DFCH	5.56E+13	168.80	−0.10931	239.3

obtained for Kissinger method are utilized in Eqs. (9) and (11). Fig. 6 (a)–(f) depicts master and experimental plots for PLA, PLA/PBS blend and their ternary nanobiocomposite with or without DCP. It can clearly be seen that PLA follows the mechanism according to the A2 and shift towards the R3 to D2 (Fig. 5a) [45]. In this type of solid-state mechanism, degradation starts from the generation of nuclei sites that acts as growth centre to initiate the thermal decomposition [36]. In general, polymer crystals have imperfections due to the presence of impurities and some point defects. These imperfections are available sites for nuclei formation. In case of PLA/PBS blend, it follows via L2 (random scission mechanism) up to 0.7 conversions, shifts slowly towards the F1 (random nucleation mechanism) at higher conversion. PLA/PBS/FCH based nanobiocomposite (with 1 wt% and 3 wt% FCH) exhibits degradation mechanism which is overlapped with A2 type mechanism at the conversion range (0.1–0.4). At $\alpha > 0.5$ degradation mechanism change towards L2 (α~0.6 to 0.7) to D2 (α~0.8) and follow D3 (α~0.9) type mechanism. For DCP treated PLA/PBS/FCH (with 1 wt% and 3 wt% FCH) nanobiocomposites, the thermal degradation proceeds via L2 (0.1–0.7) mechanism and system shift towards D3 type mechanism at higher temperature. It concerns that L2 is the rate controlling step for DCP treated PLA/PBS/FCH nanobiocomposites.

4.7. Release of gaseous product analyzed by hyphenated TGA-FTIR technique

Coupled TGA–FTIR technique is beneficial for understanding the thermal decomposition behavior of PLA/PBS blend and its nanobiocomposite [46]. In coupled TGA-FTIR technique, the intensity of IR absorbance peak related to the concentration of the release volatile components. Fig. 7 (a) – (a′) and (b) – (b′) shows the 3D and 2D IR spectrogram to detect the volatile species, related to the thermal decomposition of PLA/PBS blend and its nanobiocomposite. From the 3D plots, it could be inferred that there is no release of volatile component below 300 °C. In fact, the intensity of absorption peaks related to gaseous species emission attain its maximum at 365 °C and monotonically decreased after it which agree well with the TGA data. From the 2D stack plot, it is clear that the major decomposition product [47,48] lactide shows the absorption bands due to (stretching of C—H), (asymmetric stretching of CH_3) and (symmetric stretching of CH_3) at 3002, 2951 and 2893 cm^{-1} respectively. The band at 1792 cm^{-1}(stretching of C═O), 1377 cm^{-1} (bending of CH_3), subsequent two peaks at 1240 and 1106 cm^{-1} (stretching of C–O–C) and 930 cm^{-1} (ring skeleton). Two noteworthy bands at 1765 cm^{-1} (stretching of C═O) and 2738 cm^{-1} (stretching of –CH═O), weak bands at 2963 cm^{-1} (stretching of CH_2) and 1371 cm^{-1} (bending of CH_2), confirms that acetaldehyde is produced. Moreover, the bands appears at 2358–2310 cm^{-1} (asymmetric stretching of O═C═O), 669 cm^{-1} (bending of O═C═O) is related to carbon dioxide (CO_2) and it is produced by decarboxylation of carboxyl group during the decomposition process. The IR peaks related to carbon monoxide (CO) at 2176–2118 cm^{-1} (bending of C—O) is noticed. While the shoulder peak at 1735 cm^{-1} also confirms the release of some ester component. The FTIR spectrum of PLA/PBS/1DFCH nanobiocomposite exhibited the similar kind of main gaseous product emission. When the temperature reached around 450 °C, all the bands almost disappeared except the band of CO_2 exist till the end.

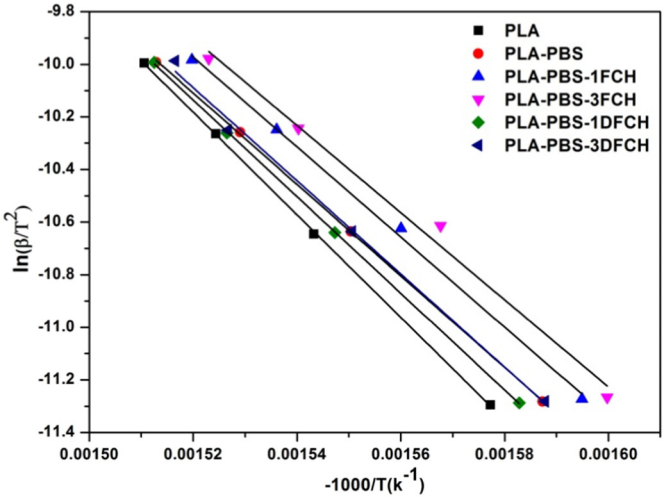

Fig. 5. Kissinger plots for PLA, PLA/PBS, and PLA/PBS/FCH nanobiocomposites with or without DCP.

4.8. Rheological behavior

Rheological analysis can ascribe a detail structural characteristic relationship of polymer and their nanobiocomposite. Therefore, the influence of FCH along with or without DCP content on the complex viscosity (η^*) of PLA/PBS system was studied. The η^* of PLA/PBS blend, PLA/PBS/FCH nanobiocomposites with or without DCP at 190 °C as a function of angular frequency (ω) are displayed in Fig. 8(a). It is noticed that PLA/PBS, PLA/PBS/1FCH, and PLA/PBS/3FCH shows the similar trend with the pseudo-Newtonian behavior whereas shear thinning started at higher ω region (≥10 rad/s). Such phenomenon is generally observed in polymer melts and the main reason is the reduction in entanglement density of the polymeric chain with the gradual increase in the value of ω. In addition, the average end to end gaps of polymeric chain segments extend at high ω region. Beyond 10 rad/s, a shear thinning behaviour of PLA/PBS blend led to lower η^* as compared to PLA/PBS ternary nanobiocomposite. After the addition of 3 wt% FCH into PLA/PBS blend, η^* is slightly lower than that of PLA/PBS/1FCH which shows shear thinning influence due to aggregation of FCH. With the addition of DCP into PLA/PBS/1FCH, the remarkable enhancement in η^* and shear thinning behaviour is exhibited, especially in the low ω region due to the formation of the interconnected network of polymeric segments and nanofillers. For PLA/PBS/1DFCH nanobiocomposite, η^* is improved significantly, taking the ω at 0.1 rad/s as a reference point, when compared with the PLA/PBS blend. Hence it is noteworthy to mention when DCP is added in PLA/PBS/1FCH, result confirms that there is possibility of PLA (presence of free radicals on tertiary C atoms) to PBS (easier abstraction of secondary hydrogen atom as compared to PLA)

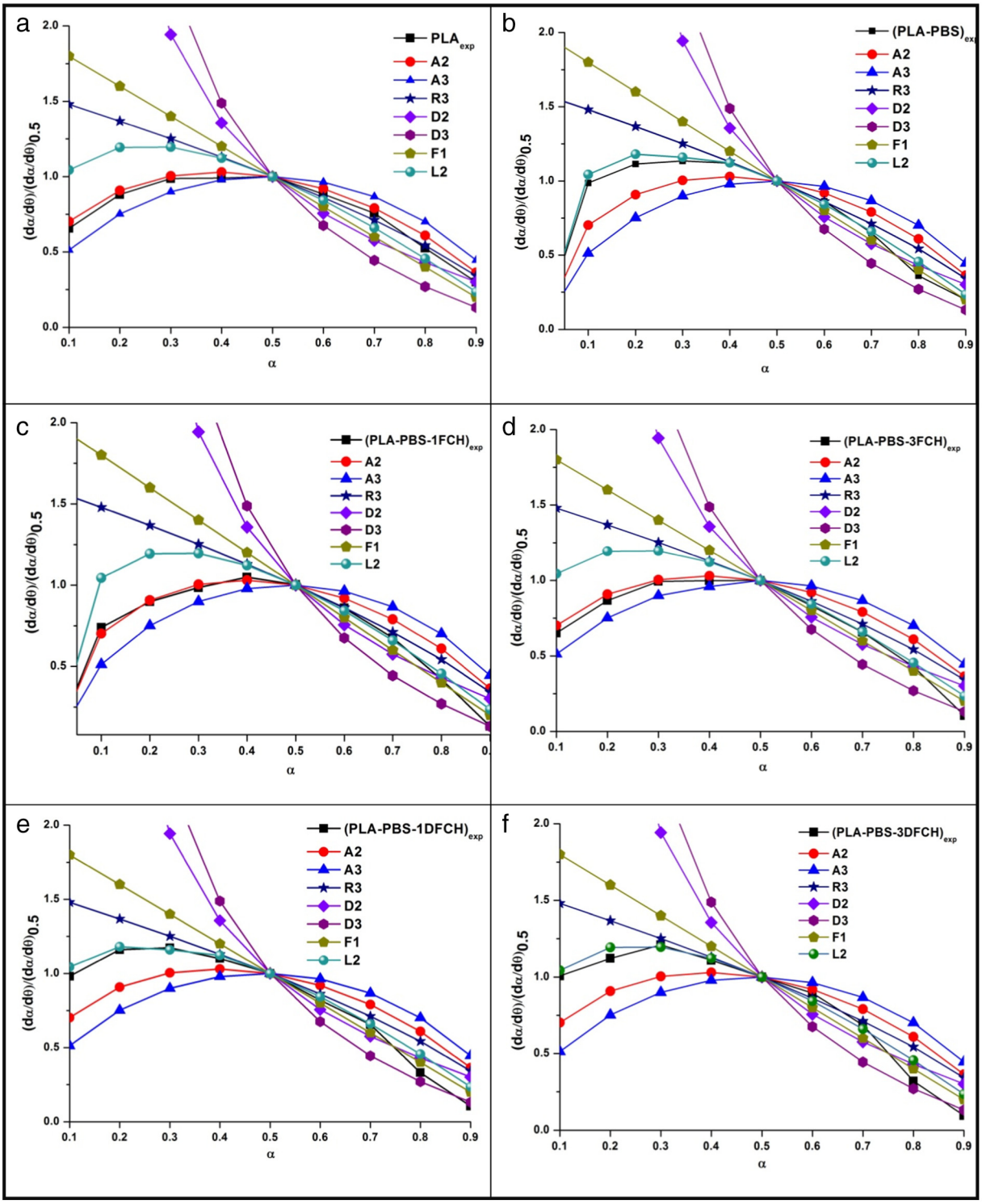

Fig. 6. Reaction mechanism obtained by the Criado method for (a) PLA (b) PLA/PBS blend, (c) PLA/PBS/1FCH, (d) PLA/PBS/3FCH, (e) PLA/PBS/1DFCH (f) PLA/PBS/3DFCH nanobiocomposites.

crosslink interaction, which subsequently leads to long chain branching, apart from free radicals generated on OLLA chains attached to FCH can also make a significant interaction with PLA and PBS segments. This significant enhancement in η^* can be related to developed long chain branching/crosslinking sites. It would produce more complex system in presence of DCP. This reaction mechanism is already mentioned in previously published articles [38]. Due to the appearance of long chain branching/crosslinking sites, polymeric segments become more connected which further restricts the mobility of individual macromolecular chains by forming more entangled structures under shear force and finally changed in flow behaviour is found [49,56]. Similar to the η^*, loss (G'') and storage (G') modulus of all samples also displayed the same trend where G'' and G' denoted the viscous region and elastic region of the melt respectively. Both G' and G'' versus ω for PLA/PBS blend and their nanobiocomposite (without DCP) is increased gradually with increasing ω, introducing terminal behaviour, as presented in Fig. 8 (b) and (c), respectively. Also for all samples, the dominance of G'' over G' at lower ω, suggested the polymeric composite are

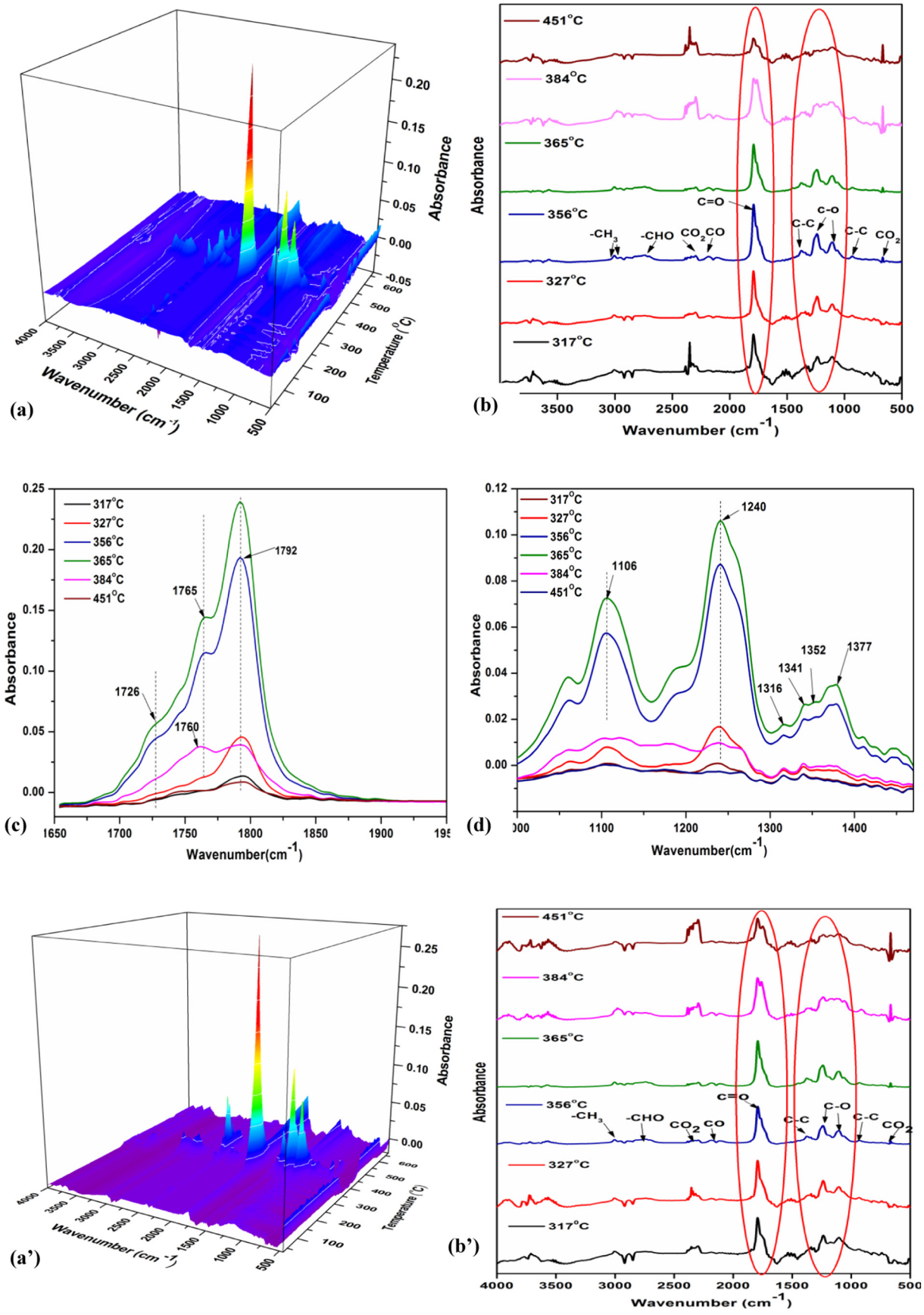

Fig. 7. 3D FTIR spectrogram (a), (a′), 2D Stack graph (b), (b′) with the enlarged image around (1650–1950 cm^{-1}) (1500–1000 cm^{-1}) (c) & (d) for the characteristic spectra of the volatile species emitted from PLA/PBS and PLA/PBS/1DFCH nanobiocomposite.

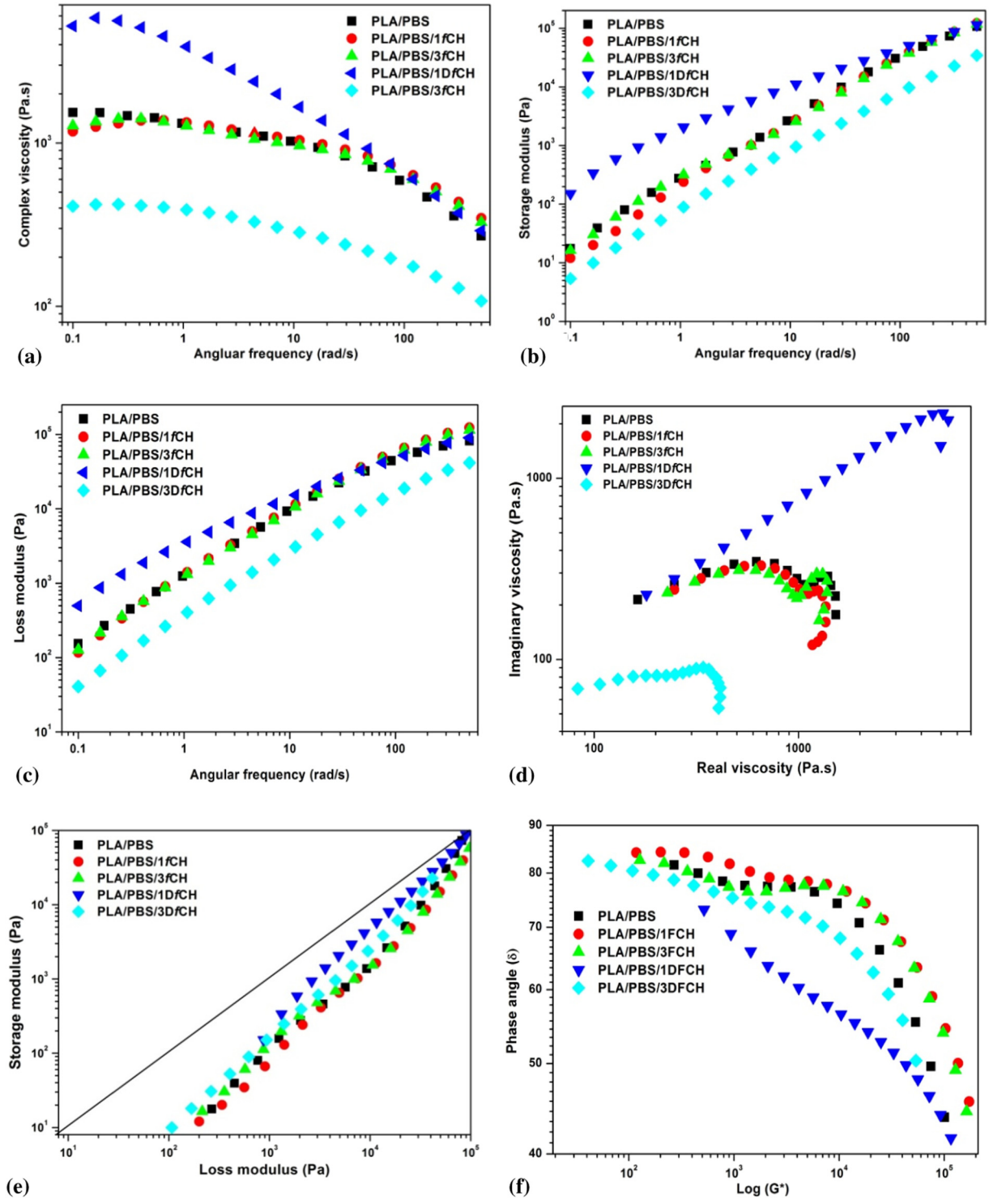

Fig. 8. Influence of modified macromolecular chains on the change of complex viscosity (Pa.s) vs angular frequency (a), storage modulus (Pa) vs angular frequency (rad/s) (b), loss modulus (Pa) vs angular frequency (rad/s) (c) Imaginary viscosity vs real viscosity (Cole-Cole graph) (d) storage modulus vs loss modulus (Han graph) (e) Phase angle vs complex modulus (Van Gurp Palmen graph) (f).

liquid like [50]. Meanwhile, the rise in G′ is emphasized, mainly at the low ω region for PLA/PBS/1DFCH which could ascribe the formation of some crosslinked/branched chains as well as the increase of the chain entanglement [53]. Moreover η, G′ and G″ were significantly dropped which suggest that the chain dissociation by shear during the melt extrusion of PLA/PBS/3DFCH. The possible reason is decrement in crosslinking efficiency which enhances the chain dissociation of the polymeric system due to presence of FCH (3 wt%) at higher content.

A logarithmic plot of real viscosity ($\eta' = G''/\omega$) versus imaginary viscosity ($\eta'' = G'/\omega$) is usually known as Cole-Cole plot to investigate the viscoelastic characteristics of the PLA/PBS, PLA/PBS/FCH in presence or absence of DCP with relaxation time distribution. It noticed that the two-phase structures in case of PLA/PBS blend. When phase separation occurred in PLA/PBS, a second semicircle found in the right side of the arc which confirmed that the second relaxation mechanism happened at the melt stage [52]. The PLA/PBS blend and their nanobiocomposites

Table 4
Influence of FCH with or without DCP content on Han plot of PLA/PBS based nanobiocomposites.

Samples	PLA/PBS	PLA/PBS/1FCH	PLA/PBS/3FCH	PLA/PBS/1DFCH	PLA/PBS/3DFCH
Slope (R^2)	1.378 (0.987)	1.361 (0.993)	1.316 (0.995)	1.229 (0.999)	1.231 (0.998)

without DCP follow the similar kind of relaxation mechanism. It found that the arc of semicircle become broad with the incorporation of DCP in PLA/PBS/1FCH nanobiocomposite which confirms that the complex structures such as branching, crosslinking and copolymers formed without phase separation [53]. All of these observations further inform that the melt strength of the PLA/PBS/1FCH system enhanced due to presence of DCP. It is noteworthy to mention that DCP modified PLA/PBS/1FCH plays a vital role to produce significant rheological characteristics. For all the samples, Han plots (log–log graph of G′ against G″) display in Fig. 8(e). Further, the diagonal line (corresponding to G′ is equal to G″) divided the plot into two portions and presented the phase transition from the viscous (when G′ < G″) to elastic (G′ > G″) response. Comparing with PLA/PBS blend, the curve of PLA/PBS/1FCH positioned at lower from the diagonal line over the entire range which confirms that the elastic contribution become smaller and further showing the decrease in elasticity of polymeric composite in melt system. With the DCP modified PLA/PBS/1FCH, the curve has to reach the diagonal line progressively and informs the higher elasticity of melt. The curve is passed across the diagonal, presuming that the crosslinked/branched structure rather than the chain extension and showed more solid-like response [54,55]. As expected, the addition of DCP with FCH into PLA/PBS decreased the value of the slope, as mention in Table 4. This shows that the topological structure of the polymeric melt is strongly affected at the transition point; the possible reason behind is the formation of branched and crosslinked structure [51,52].

To further study the topological structure of PLA/PBS blend and their composite, Van Gurp Palmen (phase angle as a function of log G*) plot depicted in Fig. 8(f) which shows that the phase angle decrease with the DCP modified PLA/PBS/1FCH in comparison of PLA/PBS blend and their nanobiocomposites. It could be due to the development of nonlinear as well as long-chain branched/crosslinked structures that limit the mobility of macromolecule.

At a given shear rate (5 s^{-1}), shear viscosity (η_τ) can be obtained as a function of time (t) to understand how the η_τ of system changes with 't' due to applied shear under the given processing condition. Shear rheological behaviors of PLA/PBS blend, PLA/PBS ternary nanobiocomposites with or without DCP are displayed in Fig. 9. It is found that η_τ decrease with 't' under the applied shear rate. At 5 s^{-1} shear rate, η_τ of PLA/PBS/FCH (1 and 3 wt%) are lower than those of PLA/PBS blend and decrease considerably with FCH content due to pro degrading character of the FCH. For DCP treated PLA/PBS/1FCH content, value of η_τ is the highest in the entire range of t, as compared to PLA/PBS blend. This can be explained due to the presence of branched/crosslinked structure, polymeric system does not experience the degradation. Further, η_τ reduced as function of t for PLA/PBS/3DFCH due to break down of polymeric system, as compared to PLA/PBS/1DFCH nanobiocomposites.

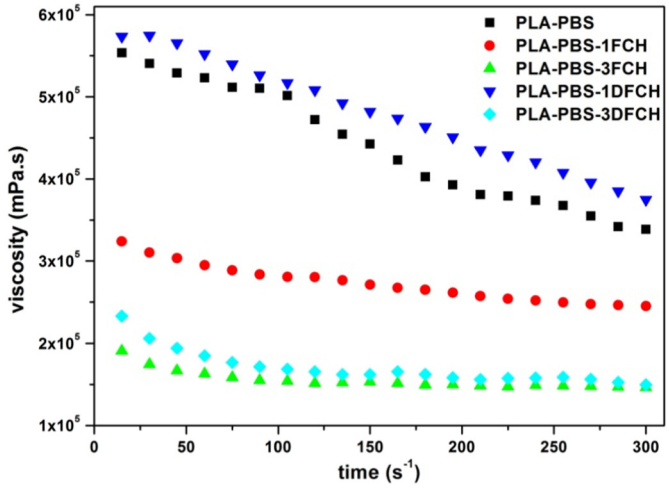

Fig. 9. Viscosity vs time graph for PLA/PBS, and PLA/PBS/FCH based nanocomposites with or without DCP.

5. Conclusion

This work reports the effect of FCH on PLA/PBS blend with and without DCP using TGA, TGA-FTIR and melt rheology analysis. TGA data shows that the thermal stability slightly improved after the incorporation of 1 wt% FCH along with DCP in PLA/PBS blend at T_{max}. This is probably due to developing crosslinking/branching sites in comparison to PLA/PBS/FCH nanobiocomposite but merely affected as compared to PLA/PBS blend. Also, non-isothermal TGA kinetics results show that apparent E_a is the highest in case of PLA/PBS/1DFCH nanobiocomposite. Based on the generalized mechanism plots, L2 → D3 mechanism proposed for DCP treated PLA/PBS/FCH based nanocomposites. Thermal release investigation performed by TGA-FTIR analysis observed that similar kinds of major volatile products released such as lactide, acetaldehyde, cyclic oligomer, CO_2, CO for PLA/PBS blend and their nanobiocomposites. The rheological study indicates that the PLA–PBS–1DFCH has shown shear thinning behavior which subsequently leads to the formation of interconnected networks of polymeric segments with FCH.

Acknowledgement

We are thankful to the Centre of Excellence for Sustainable Polymers (CoE SuSPol) funding received by the Department of Chemical and Petrochemicals, Government of India.

Appendix A. Supplementary data

Grafting by FTIR analysis (Fig. 1S); TGA profiles at four heating rate 5, 10, 15 and 20 °C (Fig. 2S); FWO plots (Fig. 3S); KAS plots (Fig. 4S); Master plots for random scission analysis (Fig. 5S). Supplementary data to this article can be found online at doi: https://doi.org/10.1016/j.ijbiomac.2019.09.058.

References

[1] C.S. Wu, Improving polylactide/starch biocomposites by grafting polylactide with acrylic acid – characterization and biodegradability assessment, Macromol. Biosci. 5 (2005) 352–361.
[2] M. Nerantzaki, G.Z. Papageorgiou, D.N. Bikiaries, Effect of nanofiller's type on the thermal properties and enzymatic degradation of poly (ε-caprolactone), Polym. Degrad. Stab. 108 (2014) 257–268.
[3] M.R. Kamal, V. Khoshkava, Effect of cellulose nanocrystals (CNC) on rheological and mechanical properties and crystallization behavior of PLA/CNC nanocomposite, Carohydr. Polym. 123 (2015) 105–114.
[4] M. Nerkar, J.A. Ramsay, B.A. Ramsay, et al., Improvements in the melt and solid-state properties of poly (lactic acid), poly-3-hydroxyoctanoate and their blends through reactive modification, Polymer 64 (2015) 51–61.
[5] W. Cherykhunthod, M. Seadan, S. Suttiruengwong, Effect of peroxide and chain extender on mechanical properties and morphology of poly (butylene succinate)/poly (lactic acid) blends, IOP Conference Series: Mater. Sci. Eng. 87 (2015), 012073.
[6] R. Muthuraj, M. Misra, A.K. Mohanty, Biocomposite consisting of miscanthus fiber and biodegradable binary blend matrix: compatibilization and performance evaluation, RSC Adv. 7 (2017) 27538–27548.
[7] L. Balau, G. Lisa, M.I. Popa, et al., Physico-chemical properties of chitosan films, Cent. Eur. J. Chem. 2 (2004) 638–647.

[8] C.-Y. Ou, C.-H. Zhang, S.-D. Li, et al., Thermal degradation kinetics of chitosan–cobalt complex as studied by thermogravimetric analysis, Carbohydr. Polym. 82 (2010) 1284–1289.
[9] K. Muraleedharan, P. Alikutty, V.A. Mujeeb, et al., Kinetic studies on the thermal dehydration and degradation of chitosan and citralidene chitosan, J. Environ. Polym, Degrad. 23 (2010) 1–10.
[10] A.K. Pal, V. Katiyar, Nanoamphiphilic chitosan dispersed poly(lactic acid) bionanocomposite bilms with improved thermal, mechanical, and gas barrier properties, Biomacromolecules 17 (2016) 2603–2618.
[11] L. Zheng, C. Li, D. Zhang, et al., Synthesis, characterization and properties of novel biodegradable multiblock copolymers comprising poly (butylene succinate) and poly (1, 2-propylene terephthalate) with hexamethylene diisocyanate as a chain extender, Polym. Int. 60 (2011) 666–675.
[12] L. Fitaroni, J. De Lima, S. Cruz, et al., Thermal stability of polypropylene–montmorillonite clay nanocomposites: limitation of the thermogravimetric analysis, Polym. Degrad. Stab. 111 (2015) 102–108.
[13] F. Carrasco, P. Pagès, J. Gámez-Pérez, et al., Kinetics of the thermal decomposition of processed poly (lactic acid), Polym. Degrad. Stab. 95 (2010) 2508–2514.
[14] D.G. Papageorgiou, E. Roumeli, K. Chrissafis, et al., Thermal degradation kinetics and decomposition mechanism of PBSu nanocomposites with silica-nanotubes and strontium hydroxyapatite nanorods, Phys. Chem. Chem. Phys. 16 (2014) 4830–4842.
[15] P. Dhar, S.P.K. Vangala, P. Tiwari, et al., Thermal degradation kinetics of poly (3-hydroxybutyrate)/cellulose nanocrystals based nanobiocomposite, J. Therm. Catal. 5 (2014) 1–7.
[16] P. Manafi, I. Ghasemi, M. Karrabi, et al., Thermal stability and thermal degradation kinetics (model-free kinetics) of nanocomposites based on poly (lactic acid)/graphene: the influence of functionalization, Polym. Bull. 72 (2015) 1095–1112.
[17] S. Ramukutty, E. Ramachandran, Reaction rate models for the thermal decomposition of ibuprofen crystals, J. Crystal. Process Technol. 4 (2014) 71–78.
[18] A. Onus, A. Aboulkas, K. Ei harif, et al., Pyrolysis of olive residue and sugar cane bagasse: non-isothermal thermogravimetric kinetic analysis, Bioresour. Technol. 102 (2011) 11234–11238.
[19] R. Valapa, S. Hussain, P.K. Iyer, et al., Influence of graphene on thermal degradation and crystallization kinetics behaviour of poly (lactic acid), J. Polym. Res. 22 (2015) 1–14.
[20] Y. Fan, H. Nishida, Y. Shirai, et al., Thermal stability of poly (l-lactide): influence of end protection by acetyl group, Polym. Degrad. Stab. 84 (2004) 143–149.
[21] P. Budrugeac, The evaluation of the non-isothermal kinetic parameters of the thermal and thermo-oxidative degradation of polymers and polymeric materials: its use and abuse, Polym. Degrad. Stab. 71 (2000) 185–187.
[22] N. Tripathi, V. Katiyar Monika, Poly (lactic acid)/modified gum arabic based bionanocomposite films: thermal degradation kinetics, Polym. Eng. Sci. 57 (2017) 1193–1206.
[23] K. Chrissafis, Detail kinetic analysis of the thermal decomposition of PLA with oxidized multi-walled carbon nanotubes, Thermochim. Acta 511 (2010) 163–167.
[24] Monika, P. Dhar, V. Katiyar. Thermal degradation kinetics of polylactic acid/acid fabricated cellulose nanocrystal based bionanocomposites. Int. J. Biol. Macromol., 104 (2017), pp. 827–836.
[25] T. Ozawa, A new method of analyzing thermogravimetric data, Bull. Chem. Soc. Jpn. 38 (1965) 1881–1886.
[26] F.J. Gotor, J.M. Criado, J. Malek, et al., Kinetic analysis of solid-state reactions: the universality of master plots for analyzing isothermal and non-isothermal experiments, J. Phys. Chem. A 104 (2000) 10777–10782.
[27] T. Ozawa, Non-isothermal kinetics and generalized time, Thermochim. Acta 100 (1986) 109–118.
[28] P.E. Sanchez-Jimenez, L.A. Perez-Maqueda, A. Perejon, J.M. Criado, Generalized kinetic master plots for the thermal degradation of polymers following a random scission mechanism, J. Phys. Chem. A 114 (2010) 7868–7876.
[29] A. Khawan, D.R. Flanagan, Solid-state kinetic models: basics and mathematical fundamentals, J. Phys. Chem. B 110 (2006) 17315–17328.
[30] A. Khawan, D.R. Flanagan, Basics and applications of solid-state kinetics: a pharmaceutical perspective, J. Pharm. Sci. 95 (2006) 472–498.
[31] S. Mallakpour, M. Taghavi, Kinetics and thermal degradation study of optically active and thermally stable aromatic polyamides with flame-retardancy properties, Polym. J. 41 (2009) 308–318.
[32] J. Ambrosio-Martín, M.J. Fabra, A. Lopez-Rubio, et al., An effect of lactic acid oligomers on the barrier properties of polylactide, J. Mater. Sci. 49 (2014) 2975–2986.
[33] S. Luo, J. Cao, A.G. McDonald, Interfacial improvements in a green biopolymer alloy of poly(3-hydroxybutyrate-co-3-hydroxyvalerate) and lignin via in situ reactive extrusion, ACS Sustain. Chem. Eng. 4 (2016) 3465–3476.
[34] P. Dhar, D. Tarafder, A. Kumar, et al., Thermally recyclable poly lactic acid/cellulose nanocrystal films through reactive extrusion process, Polymer 87 (2016) 268–282.
[35] I.E. Yuzay, R. Auras, H. Soto-Valdez, et al., Effects of synthetic and natural zeolites on morphology and thermal degradation of poly(lactic acid) composites, Polym. Degrad. Stab. 95 (2010) 1769–1777.
[36] F.D. Kopinke, M. Remmler, K. Mackenzie, et al., Thermal decomposition of biodegradable polyester-II. Poly(lactic acid), Polym. Degrad. Stab. 53 (1996) 329–342.
[37] M. Tesfaye, R. Patwa, R. Kommadath, et al., Silk nanocrystals stabilized melt extruded poly (lactic acid) nanocomposite films: effect of recycling on thermal degradation kinetics and optimization studies, Thermochim. Acta 643 (2016) 41–52.
[38] A.K. Pal Monika, S.M. Bhasney, et al., Effect of dicumyl peroxide on a poly (lactic acid) (PLA)/poly (butylene succinate)/functionalized chitosan based nanobiocomposite for packaging: a reactive extrusion study, ACS Omega 3 (2018) 13298–13312.
[39] J.P. Mofokeng, A.S. Luyt, Morphology and thermal degradation studies of melt-mixed poly (lactic acid) (PLA)/poly (ε-caprolactone) (PCL) biodegradable polymer blend nanocomposite with TiO_2 as filler, Polym. Test. 45 (2015) 93–100.
[40] R. Valapa, G. Pugazhenthi, V. Katiyar, Thermal degradation kinetics of sucrose palmitate reinforced poly (lactic acid) biocomposites, Int. J. Biol. Macromol. 65 (2014) 275–283.
[41] J. Li, W. Zheng, L. Li, et al., Thermal degradation kinetics of g-HA/PLA composite, Thermochim. Acta 493 (2009) 90–95.
[42] H. Zou, C. Yi, L. Wang, et al., Thermal degradation of poly (lactic acid) measured by thermogravimetry coupled to fourier transform infrared spectroscopy, J. Therm. Anal. Calorim. 97 (2009) 929–935.
[43] L. Wei, N.M. Stark, A.G. McDonald, Interfacial improvements in biocomposites based on poly (3-hydroxybutyrate) and poly (3-hydroxybutyrate-co-3-hydroxyvalerate) bioplastics reinforced and grafted with α-cellulose fibers, Green Chem. 17 (2015) 4800–4814.
[44] S. Tiptipakorn, S. Damrongsakkul, S. Ando, et al., Thermal degradation behaviours of polybenzoxazine and silicon-containing polyimide blends, Polym. Degrad. Stab. 92 (2007) 1265–1278.
[45] G.Z. Papageorgiou, D.S. Achilias, S. Nanaki, et al., PLA nanocomposites: effect of filler type on non-isothermal crystallization, Thermochim. Acta 511 (2010) 129–139.
[46] C.A. Wilkie, TGA/FTIR: an experimental useful technique for studying polymer degradation, Polym. Degrad. Stab. 66 (1999) 301–306.
[47] C. Vogel, H.W. Siesler, Thermal degradation of poly (ε-caprolactone), poly (l-lactic acid) and their blends with poly (3-hydroxy-butyrate) studied by TGA/FT-IR spectroscopy, Macromol. Symp. 265 (2008) 183–194.
[48] N. Tudorachi, R. Lipsa, F.R. Mustata, Thermal degradation of carboxymethyl starch–g-poly (lactic acid) copolymer by TG–FTIR–MS analysis, Ind. Eng. Chem. Res. 51 (2012) 15537–15545.
[49] Y.-S. He, J.-B. Zeng, G.-C. Liu, et al., Super-tough poly (l-lactide)/crosslinked polyurethane blends with tunable impact toughness, RSC Adv. 4 (2014) 12857–12866.
[50] M. Tesfaye, R. Patwa, A. Gupta, et al., Recycling of poly (lactic acid)/silk based bionanocomposites films and its influence on thermal stability, crystallization kinetics, solution and melt rheology, Int. J. Biol. Macromol. 101 (2017) 580–594.
[51] D. Ji, Z. Liu, X. Lan, et al., Morphology, rheology, crystallization behaviour, and mechanical properties of poly (lactic acid)/poly (butylene succinate)/dicumyl peroxide reactive blends, J. Appl. Polym. Sci. 131 (2014) 39580–39588.
[52] C. Zhang, Y. Huang, C. Luo, et al., Enhanced ductility of polylactide materials: reactive blending with pre-hot sheared natural rubber, J. Polym. Res. 20 (2013) 2–9.
[53] M. Tesfaye, R. Patwa, P. Dhar, et al., Nanosilk-grafted poly (lactic acid) films: influence of cross-linking on rheology and thermal stability, ACS Omega 2 (2017) 7071–7084.
[54] J. Cai, A. Wirasaputra, Y. Zhu, et al., The flame retardancy and rheological properties of PA6/MCA modified by DOPO-based chain extender, RSC Adv. 7 (2017) 19593–19603.
[55] B. Zhang, X. Bian, D. Zhou, et al., Toughening modification of PLLA by combination of copolymerization and in situ reactive blending, RSC Adv. 6 (2016) 113366–113376.
[56] Y. Huang, C. Zhang, Y. Pan, et al., Study on the effect of dicumyl peroxide on structure and properties of poly (lactic acid)/natural rubber blend, J. Polym. Environ. 21 (2013) 375–387.
[57] R. Al-Itry, K. Lamnawar, A. Maazouz, Improvement of thermal stability, rheological and mechanical properties of PLA, PBAT and their blends by reactive extrusion with functionalized epoxy, Polym. Degrad. Stab. 97 (2012) 1898–1914.
[58] S.Y. Gu, K. Zhang, J. Ren, et al., Melt rheology of polylactide/poly (butylene adipate co terephthalate) blends, Carbohydr. Polym. 74 (2008) 79–85.
[59] P. Srimalanon, B. Prapagdee, T. Markpin, et al., Effects of DCP as a free radical producer and HPQM as a biocide on the mechanical properties and antibacterial performance of in situ compatibilized PBS/PLA blends, Polym. Test. 67 (2018) 331–341.